Journal of Geophysical Research: Atmospheres

RESEARCH ARTICLE
10.1029/2017JD027650

Multiscale processes in the genesis of a near-equatorial tropical cyclone during the Dynamics of the MJO Experiment: Results from partial lateral forcing experiments

Hongwei Yang[1] and **Bin Wang**[2,3]

[1]APEC Climate Center, Busan, South Korea, [2]Earth System Modeling Center, Nanjing University of Information Science and Technology, Nanjing, China, [3]Department of Atmospheric Sciences and International Pacific Research Center, University of Hawaii at Manoa, Honolulu, HI, USA

Key Points:
- The MJO forcing favors the development of TC05A, while the lateral forcings from synoptic and interannual variations play a minor role
- Interaction between the MJO and northeast winter monsoon has the greatest impact on the genesis location and path of TC05A
- The partial lateral forcing (PLF) method is an effective tool to identify the key factors controlling the extreme events

Correspondence to:
H. Yang,
hwyangapcc@gmail.com

Citation:
Yang, H., & Wang, B. (2018). Multiscale processes in the genesis of a near-equatorial tropical cyclone during the Dynamics of the MJO Experiment: Results from partial lateral forcing experiments. *Journal of Geophysical Research: Atmospheres*, *123*. https://doi.org/10.1029/2017JD027650

Received 24 AUG 2017
Accepted 22 APR 2018
Accepted article online 4 MAY 2018
Corrected 4 JUN 2018

This article was corrected on 4 JUN 2018. See the end of the full text for details.

Abstract Tropical cyclone (TC) 05A (TC05A, November 2011) over the Indian Ocean originated near the equator and brought huge damages to Sri Lanka and India. The genesis and propagation of TC05A involves interactions with the Madden–Julian Oscillation (MJO), interannual (IA) variations, and other synoptic (SY) systems. To investigate the impacts of the SY, MJO, and IA forcings across the lateral boundaries on TC05A, regional simulation with the Weather Research and Forecast model through the partial lateral forcing approach is conducted. The control experiment reproduces realistic genesis and movement of TC05A and associated heavy rainfall, as well as the mean states and MJO. Both the SY and IA forcings make a moderate contribution to the initiation of cyclonic vorticity and rainfall enhancement in the central Indian Ocean and moderate modification of the TC05A track. However, it is the MJO forcing that fundamentally reproduces a coherent moist, low-level convergence, and a cyclonic environment that is favorable for the development of TC05A. The greatest impact of northern boundary intraseasonal (IS) forcing on the genesis location and path of TC05A is further identified, suggesting the importance of the interaction between the MJO and northeast winter monsoon. In contrast, the southern boundary IS forcing is unimportant and the western and eastern boundary IS forcings play a moderate role in slowing down TC05A and modifying its track, intensity, and rainfall. This study demonstrates that the partial lateral forcing method is an effective tool to identify the key factors controlling the extreme events through regional climate modeling.

1. Introduction

On 26 November 2011, a near-equatorial tropical cyclone (TC) 05A (TC05A) damaged 5,700 homes and caused 19 deaths in Sri Lanka. The India Meteorological Department identified the storm and upgraded it on 28 November to a deep depression with maximum sustained winds of 65 km/hr (Moum et al., 2014). TC05A is a well-observed, very interesting case of the Madden–Julian Oscillation (MJO)-TC interaction during the Intensive Observing Period of the Dynamics of the MJO (DYNAMO) field campaign (Fu et al., 2013; Gottschalck et al., 2013).

TC05A occurred during a moderate La Niña and a positive Indian Ocean (IO) Dipole (IOD) event (Gottschalck et al., 2013; Yoneyama et al., 2013). The IOD peaked in October with positive (negative) sea surface temperature (SST) anomaly (SSTA) over the western (eastern) IO. The IOD is accompanied by an oceanic eastward Wyrtki jet that is phase locked to the monsoon transition season, which transports anomalous warm water from the western to eastern IO (McPhaden et al., 2015). The moderate La Niña induced westerly over the equatorial IO (Lau & Nath, 2003) to enhance the eastward Wyrtki jet. The eastward oceanic currents balanced the zonal tilt of thermocline induced by the IOD, which resulted in the zonally flattened equatorial thermocline that persisted from October to November. Therefore, the warmest SST (29–30 °C) with positive SSTA sustained over the equatorial IO east of 60°E with the zonally flat thermocline during November 2011. The positive anomalies of convection and humidity over the equatorial IO occurred in November (Gottschalck et al., 2013) as a response to the positive SSTA. This coherent large-scale air-sea environment would favor the development of MJO convective envelope (Fu et al., 2015; Woolnough et al., 2001) and TC genesis.

TC05A took place during a prominent MJO event. The MJO is the dominant mode of tropical convective variability on the intraseasonal (IS) time scales (Madden & Julian, 1994). The associated circulation systems propagate eastward as a Rossby-Kelvin wave couplet (Wang & Rui, 1990). Studies have shown that the MJO modulates TC activity over each basin on its eastward journey (e.g., Fu & Hsu, 2011; Fudeyasu et al., 2010;

Hall et al., 2001; Huang et al., 2011; Liebmann et al., 1994; Maloney & Hartmann, 2000; Schreck et al., 2012; Wang & Zhou, 2008). The MJO impacts TC through changing the environmental vertical wind shear (Mo, 2000), low-level cyclonic vorticity and meridional wind shear (Bessafi & Wheeler, 2006; Hall et al., 2001), and relative humidity (Klotzbach, 2010). Xu et al. (2014) found that the IS oscillation exerts both a direct and an indirect impact on TC genesis. The direct impact is through the increase of background low-level cyclonic vorticity and moisture, and the indirect impact is through the modulation of the synoptic wave train. Wu and Duan (2015) suggested that synoptic wave trains in the monsoon trough over the western North Pacific can develop in the low-frequency background without high-frequency signals. The cyclonic circulation of the wave train provides low-level synoptic disturbances for TC genesis. Camargo et al. (2009) applied the genesis potential index established by Emanuel and Nolan (2004) to quantitatively diagnose the contributions of four large-scale factors to TC genesis. Those large-scale factors include vertical wind shear, midtropospheric relative humidity, maximum potential intensity, and 850-hPa absolute vorticity. Wang and Moon (2017) found that the factors controlling climatological TC genesis are not all applicable to the IS time scale. They showed that the most effective factors controlling IS TC genesis are 850-hPa relative vorticity (ζ_{850}) weighted by the Coriolis parameter, $f\zeta_{850}$, and 500 hPa vertical motion ($f\omega_{500}$). The total vertical wind shear and maximum potential intensity is unimportant, and the role of 600 hPa relative humidity is very well represented by ω_{500}. It was suggested that any form of low-frequency (relative to TC), large-scale variability that alters the dynamical factors favorable for cyclogenesis could also modulate TC activity (Lau & Waliser, 2012).

During the TC05A period from 23 to 30 November including its pre-TC disturbance stage, there were a number of other synoptic disturbances, including two convectively coupled mixed Rossby-Gravity (MRG)-like waves and equatorial Rossby (ER) wave gyres. TC activity can be modulated by ER waves (Bessafi & Wheeler, 2006). The interactions among the equatorial modes may also modulate the TC genesis. Zong and Wu (2015) suggested that the synoptic TC precursor disturbances enhance the midlevel and low-level relative vorticity and convergence by establishing a limited, rotation-dominant area but contribute little to reducing vertical wind shear. Aiyyer and Molinari (2003) suggested that a MRG wave can produce small-scale, off-equatorial eddies which could serve as seedlings for TC when it meets an equatorial asymmetric large-scale heating of the MJO. Indeed, a sequence of TC geneses in this way is not uncommon (Dickinson & Molinari, 2002). Schreck (2015) found that the onset of vorticity anomalies that generate TC occurs with the Kelvin wave passage, while the MJO apparently establishes the duration of these anomalies. Chen and Chou (2014) found that the joint contribution from more than one wave type favors the creation of a coherent environment with enhanced low-level cyclonic vorticity, horizontal convergence, or vertical easterly shear in a preferred region. Hogsett and Zhang (2010) found that the MJO, together with a convectively coupled Kelvin wave, provides the necessary low-level convergence and rotation for the development of TC. Gottschalck et al. (2013) showed that the interaction of the convective phases of an ER or a tropical depression (TD)-like wave, a Kelvin wave, and the MJO leads to the genesis of TC05A.

Although previous studies have recognized the role of multiscale interactions among the convectively coupled equatorial modes in the genesis of TC, the scale-interactive processes among synoptic (SY) disturbance, the MJO and interannual (IA) variation, which result in the genesis of TC05A, still remain mysterious. For example, what is the necessary perturbation that brings about the genesis of TC05A? What makes TC05A pass Sri Lanka and the southern tip of India? We are motivated to address these questions here through the partial lateral forcing (PLF) (Yang & Wang, 2015) experiments with the Weather Research and Forecast (WRF) model (Skamarock et al., 2008). Our study aims to better understand the roles of the multiscale lateral forcing in the near-equatorial genesis and track of TC05A.

2. Model and Numerical Experimental Design

The WRF model version 3.5 (Skamarock et al., 2008), a nonhydrostatic model using sigma coordinates, is used in this study. The main physical options we use are Thompson microphysics scheme (Thompson et al., 2008), the Yongsei University planetary boundary layer scheme (Hong et al., 2006), the Betts-Miller-Janjic cumulus parameterization (Janjic, 1994, 2000), the shortwave and longwave radiation schemes which are based on the Community Atmospheric Model (CAM) 3 (Collins et al., 2004), and the unified Noah land-surface model (Chen & Dudhia, 2001).

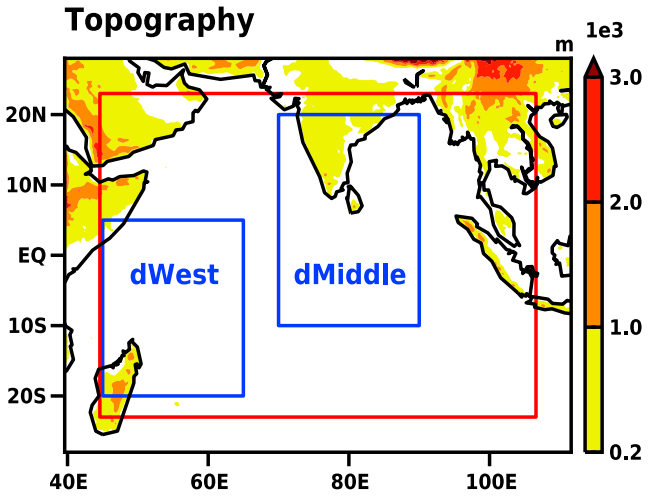

Figure 1. Model domain (28°S–28°N, 39.6°–111.6°E) and topography (color shadings in units of meters). Topographic contours of 1,000, 2,000, and 3,000 m are highlighted. The rectangular boxes marked by blue lines refer to the regions of dWest (20°S–5°N, 45°–65°E) and dMiddle (10°S–20°N, 70°–90°E). Buffer zone is outside of the red box (23°S–23°N, 44.6°–106.6°E).

To consider the regional climate regime, the control (CTL) experiment requires a sufficiently large domain size, with which the regional model can develop its own dynamics and availability of sufficient computational resources. The model domain that we design covers a large portion of the IO, extending from 28°S to 28°N and from 39.6°E to 111.6°E (Figure 1). We choose the cylindrical equidistant map projection, as the grid is close to rectangular in Euclid space over the tropical region. The zonal and meridional grid space is chosen approximately as of 20 km in order to resolve a TC. The model has 375 west–east and 323 south–north grid points, and 37 sigma layers up to 50 hPa in the vertical direction.

The CTL experiment starts from 18Z 3 November to 00Z 1 December 2011, which is initially and laterally forced by the European Centre for Medium-Range Weather Forecasts Reanalysis (ERA)-Interim reanalysis data set (Dee et al., 2011). The ERA-Interim reanalysis data set is available at 6-hr intervals with a horizontal resolution of 0.75° and 37 pressure levels. The forcing fields include geopotential height, air temperature, specific humidity, and horizontal winds. The width of the buffer zone is set to be 25 grid points, where the prognostic variables of the WRF model are nudged toward the large-scale forcing fields of ERA-Interim. The initial states on all pressure levels are the geopotential height, air temperature, specific humidity, and horizontal winds from ERA-Interim. Other initial conditions include surface pressure, sea-level pressure, 2-m height moisture, 2-m height temperature, 10-m height horizontal winds, soil moisture, soil temperature, and skin temperature. The 6-hourly varying skin temperature over the ocean is considered as SST. Surface skin temperature over land is updated using the unified Noah land-surface model (Chen & Dudhia, 2001).

To study the effects of SY, IS, and IA forcings at the lateral boundary (LB) on TC genesis, intensification, and movement, we design the sensitivity experiments based on the PLF methodology, which has been used to study the devastating rainfall in the Asia Monsoon region (Yang & Wang, 2015). The details of the PLF methodology is as follows:

1. Decomposition of the LB condition.
   a. First, calculate the climatological daily mean (CDM) data averaged for the period from 1979 to 2013.
   b. Second, the climatological annual cycle (CAC) is obtained by calculating 31-day running mean CDM.
   c. Third, the daily mean anomaly (DMA) is obtained by subtracting the CAC from the daily mean (DM) data.
   d. Fourth, the IA component is obtained by calculating 365-day running mean over the DMA.
   e. Fifth, the (SY + IS) field is obtained by subtracting the IA component from the DMA.
   f. Finally, the IS component is further separated from the SY by calculating 5-day running mean over the (SY + IS) field.

The above calculation is carried out on each field of humidity, temperature, horizontal wind *u*, horizontal wind *v*, and geopotential height of ERA-Interim reanalysis. Then we have the SY, IS, and the IA variations of those five fields. All the SY, IS, and IA variations are derived from ERA-Interim based on the period of 1979–2013. The SY and IS are slightly correlated over some areas along the LB (figure not shown). Atmospheric variables have a feature that the low-frequency variations are clearly separated but not the high-frequency variations. Thus, it is difficult to clearly separate the IS and SY components using most digital filters that basically involved convolution calculations. One can use alternative band-pass filter or harmonic analysis to separate the forcing on different time scales. The results are essentially the same (Zhang et al., 2017).

2. First three sensitivity experiments are named as Exp_noSY, Exp_noIS, and Exp_noIA, in which the SY, IS, and IA variations are respectively removed from the LB forcing of the CTL experiment. The initial values at the surface in the three experiments are kept the same as in the CTL experiment, whereas on each pressure level the corresponding SY, IS, and IA are separately removed from the total fields of the initial variables. Note that the total field of each LB variable is the sum of diurnal cycle, SY, IS, IA, and AC. This study only focuses on the impacts of SY, IS, and IA on the TC05A.

3. To further identify the role of the IS forcing across each side of the LB, the IS forcing is separately removed from the eastern, southern, western, and northern LBs in four additional sensitivity experiments based on the CTL experiment, and are named as Exp_EnoIS, Exp_SnoIS, Exp_WnoIS, and Exp_NnoIS, respectively.

In all the experiments, our analysis mainly focuses on the MJO active phase from 15 to 30 November, which covers the lifespan of TC05A. The physical parameterizations and model configuration are kept the same for all the experiments. Satellite rainfall of the Climate Prediction Center Morphing Technique (CMORPH) (Joyce et al., 2004) and ERA-Interim circulation fields are used to verify the results of the CTL experiment.

3. Performance of the Control Experiment

To verify the model's ability in representing the interaction between TC05A and the MJO, we first assess performances of the CTL experiment, including the mean states, the MJO, SY disturbances, and TC genesis and propagation.

3.1. Mean Circulation

Figure 2 compares the low-level mean circulation (geopotential height and horizontal winds at 850 hPa) between ERA-Interim and the CTL experiment from 15 to 30 November. In the ERA-Interim analysis the low-level boreal winter northeasterly monsoon prevails across the Indian subcontinent and the Arabian Sea; after crossing the equator, the boreal winter monsoon flows become northwesterly winds, meeting with the southeast trades of the Southern Hemisphere (SH) and forming the southwestern IO (SWIO) convergence zone in the equatorial region. The easterlies on the northern flank of the Mascarene High enhance the trade winds toward the African coast. On the equator, strong westerly exists.

In the CTL experiment, the mean northern IO monsoon flows, the southern IO trades, and the SWIO convergence zone are all reasonably reproduced. The simulated northern Rossby gyre shifts southwestward and the southern gyre shifts westward; thus, the path of the strong low-level westerly is twisted, which is also evidenced by the contrast of the underestimated geopotential height close to the African coast and the overestimated height to its east in the bias map (Figure 2c). Moreover, the CTL experiment overestimates the geopotential height along the eastern boundary of the domain (Figure 2c).

Comparison between the observed and simulated mean precipitation is shown in Figures 2d and 2e. Generally, a broad rainfall band over the equatorial IO is reasonably simulated in the CTL experiment. A large area of heavy rainfall over the central IO (Figure 2d) is well simulated in the CTL experiment except that the simulated intensity is larger. The narrow rain belt extending northwestward from the precipitation center along the western coast of India indicates the path of TC05A, which is correctly simulated almost during the whole TC lifespan except that the rainfall is too weak when TC05A reaches 20°N. The SH rainfall maxima in the observation along the line from the southern Rossby gyre to the central IO and Sumatra resemble the SWIO convergence zone. But the CTL experiment underestimates (overestimates) rainfall associated with the SWIO convergence zone over the western and eastern IO (central IO). Two rainfall centers corresponding to the Rossby gyres are clearly reproduced in the CTL experiment except that the intensity of the northern (southern) gyre is overestimated (underestimated). Overall, the spatial correlation of mean precipitation in the CTL experiment relative to CMORPH is 0.68 and that relative to ERA-Interim precipitation is 0.84 (figure not shown).

3.2. The MJO Event

Figures 3a and 3b compare the Hovmoller diagram of rainfall associated with the MJO between CMORPH and the CTL experiment. The correlation coefficient is 0.52 between the simulated and observed pattern during the period from 5 to 28 November, suggesting that the MJO is reasonably captured in the CTL experiment. During the MJO suppressed phase, the CTL experiment prolongs the rainfall associated with the previous MJO event, which produces a wet bias compared with CMORPH data. The MJO active phase starts around 15 November over the IO near the African coast. The CTL experiment slightly overproduces precipitation in the beginning, which is consistent with the bias in the simulated Rossby gyres and the corresponding rainfall in Figures 2b and 2e. The CTL experiment also produces more precipitation around 80°E than CMORPH in the early stage.

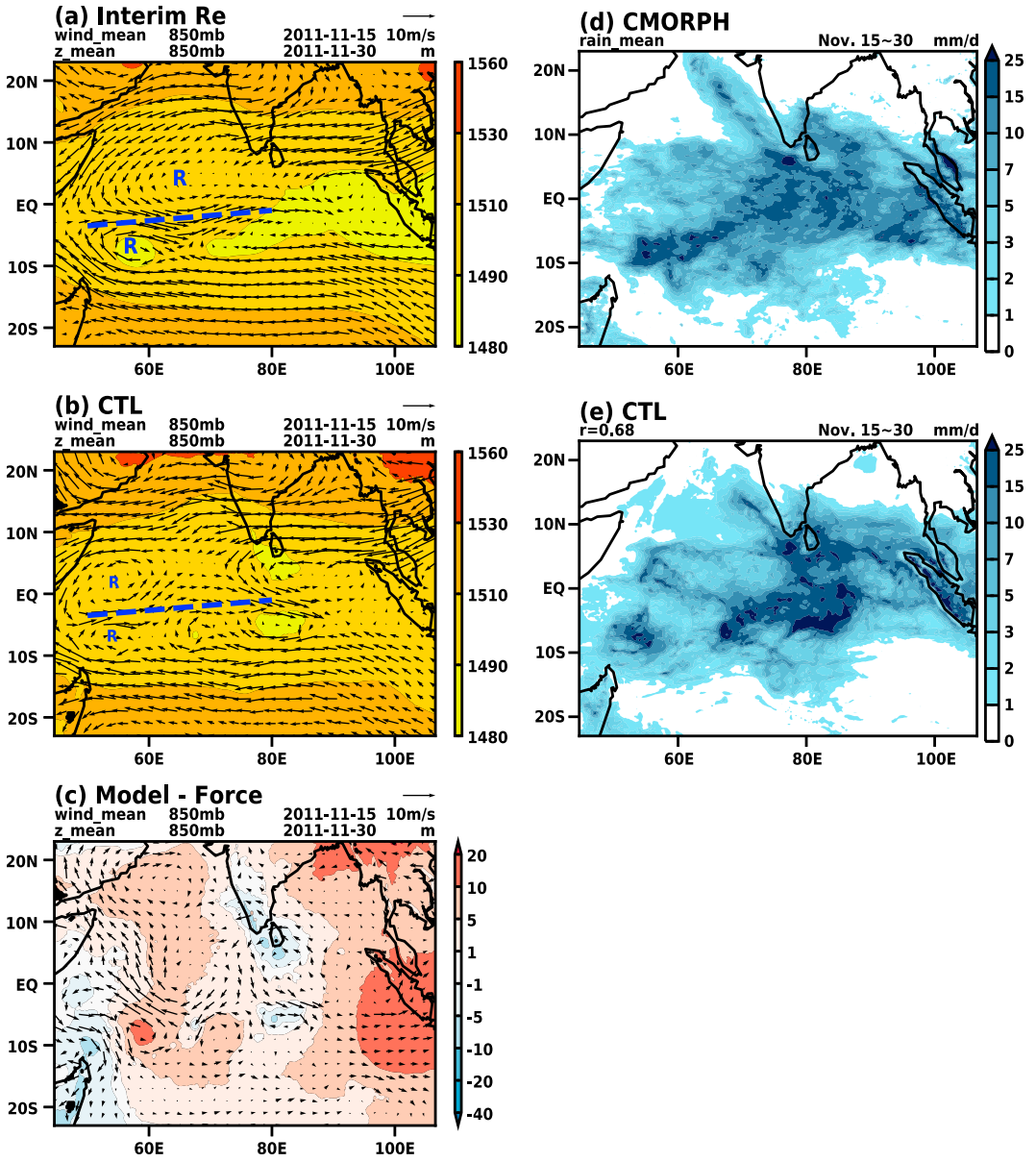

Figure 2. (a and b) The mean geopotential height (shading in units of meter) and horizontal winds (vector in units of m/s) at 850 hPa during 15–30 November from ERA-Interim reanalysis data and its forced control (CTL) experiment, respectively. (c) The bias of the CTL experiment defined as the departure of (b) from (a). (d and e) The mean rainfall (shading in units of mm/day) during the same period from satellite observation of CMORPH and the CTL experiment, respectively. Letter "R" in (a) and (b) denotes equatorial Rossby gyres associated with the Madden–Julian oscillation. Dashed blue line illustrates the southwestern Indian Ocean convergence zone. Black masked area is the area where the topography is higher than 850 hPa. CMORPH = Climate Prediction Center Morphing Technique.

3.3. Synoptic Precipitation

Figure 4 displays the simulated areal-averaged rainfall events. The region dWest (Figure 1) is the initial location of the MJO. CMORPH shows three rainfall peaks during the MJO event (Figure 4a). The first peak on 17 November is caused by the intensification of the SWIO convergence zone, which indicates that the beginning of the westerly wind burst (WWB) developed from the cross-equatorial monsoon flow adjusted by the cyclonic cells in the SWIO convergence zone (figure not shown). The second event on 21 November is caused by the formation of a pair of Rossby gyres (whose two cell centers are not at the same longitude), of which the westerly flow generates strong convergence in the dWest. The third event on 25 November is mainly caused

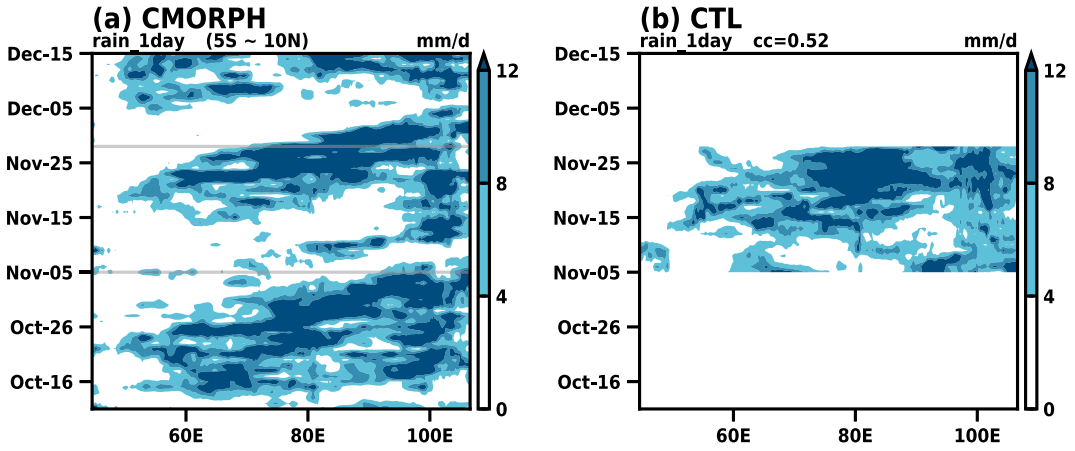

Figure 3. Time-longitude cross sections of daily precipitation (mm/day) averaged over the tropical IO between 5°S and 10°N, which are derived from (a) satellite data CMORPH, and (b) control (CTL). In order to clearly exhibit the November Madden–Julian oscillation event in a background, the processes before and after that event are also shown in (a). The pattern correlation coefficient is 0.52 between (a) and (b) during 5–28 November. CMORPH = Climate Prediction Center Morphing Technique.

by the southern Rossby gyre in the dWest, which is coupled with TC05A and rapidly intensified together with it. The CTL run captures the three events reasonably well except that it underestimates the rainfall amount in the second and third events. The correlation between CMORPH and the CTL simulation is 0.72.

Figure 4b compares the rainfall in CMORPH data set and simulated in the CTL run in the region dMiddle, where TC05A is formed. There is light rainfall before 23 November. The rainfall rapidly increases after the

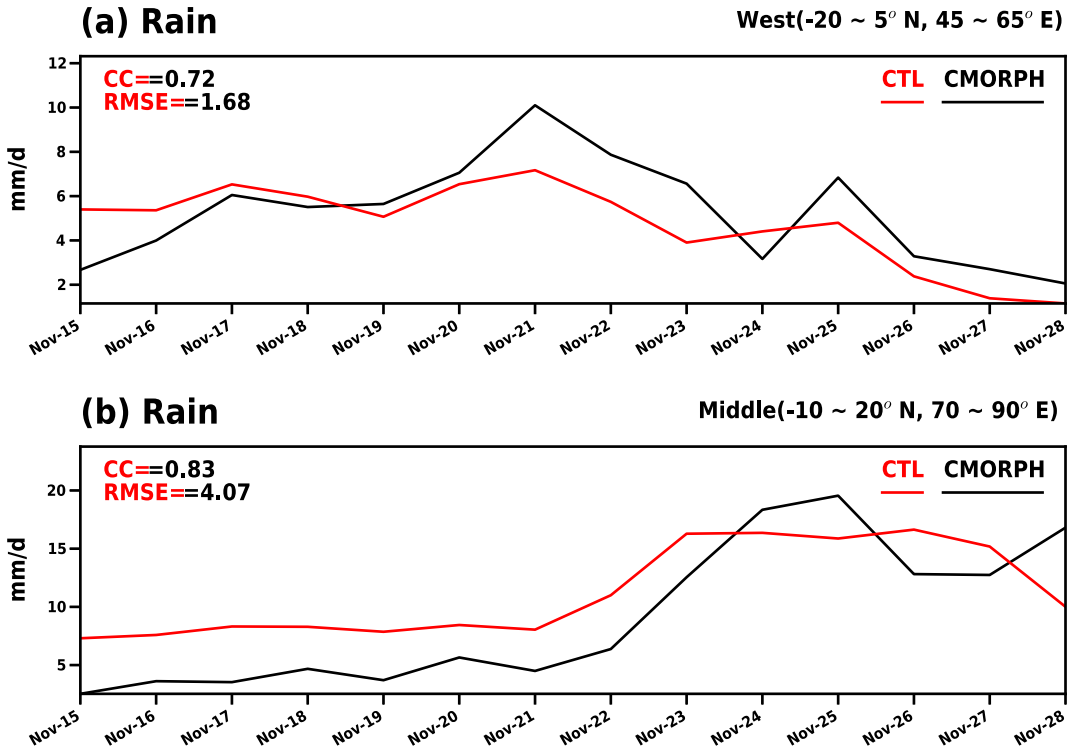

Figure 4. The satellite-observed (CMORPH, black) and simulated (CTL, red) area-averaged daily precipitation (mm/day) from 15 to 28 November 2011, over the (a) dWest and (b) dMiddle (see Figure 1 for definition). The correlation coefficients and root-mean-square errors are indicated in the top left corner of each panel. CTL = control; RMSE = root-mean-square error. CMORPH = Climate Prediction Center Morphing Technique.

genesis of TC05A on 23 November. The rapid intensification of TC05A on 24 and 25 November causes the maximum rainfall in the dMiddle. Here we define the rapid intensification as an increase of more than 6 knots in the maximum sustained 10-m wind speed over a period of 12 hr or less. Since 26 November, TC05A begins to cross the west boundary of the dMiddle, which decreases the areal rainfall. Generally, the CTL run reasonably captures the rainfall variations except that the CTL run overestimates the rainfall in the early stage while it underestimates the rainfall when TC05A reaches its peak. The correlation between CMORPH and the CTL simulation is 0.83.

3.4. Genesis, Intensity, and Movement of TC05A

Figure 5 exhibits daily evolution of the low-level circulation during the lifespan of TC05A. On 23 November, ERA-Interim shows a closed MRG-like gyre at the southern tip of India, which is the seed of TC05A (Figure 5a). Another feature is a pair of Rossby gyres straddling the equator in the western IO with the southern gyre being suppressed. To the east of that suppressed gyre, there is a cyclonic disturbance which connects with the equatorial westerly and encounters the northeasterly of the MRG-like vortex. Therefore, a strong convergence region is formed on the equator around 70°E, which produces a heavy rainfall center (figure not shown). The CTL run realistically reproduces the locations of the Rossby and MRG-like gyres (Figure 5d). On 24 November, the MRG-like vortex moves northwestward and becomes an off-equatorial TD (or TC05A) in both the observation and the CTL run. Meanwhile, the southern Rossby gyre and the WWB are also obviously strengthened in both the observation and the CTL run. On 25 November, TC05A (or TD) is rapidly intensified, and both Rossby gyres and the WWB associated with the MJO are also strengthened in the observation. The CTL run underestimates (overestimates) the intensity of the Rossby gyres (TC05A). On 26 November, TC05A further intensifies and moves northwestward and joins the northern Rossby gyre in the observation, while a second MRG-like gyre forms on the equator southeast to TC05A. The CTL run reasonably reproduces TC05A and the new MRG-like gyre, but the Rossby gyres shift westward. On 27 November, TC05A continues to move northwestward and the second MRG-like gyre is strengthened. The location of TC05A is reasonably captured in the CTL run. The second MRG-like gyre shifts southward and becomes a TD-type disturbance in the CTL run. On 28 November, the observed TC05A moves farther northwestward; the second MRG-like gyre moves to the SH and becomes a TD-type disturbance. Meanwhile, a new (third) MRG-like gyre forms on the equator west of Sumatra. The CTL run simulates well the main features including the genesis and northwestward movement of TC05A, the TD-type disturbance over the SH, and the occurrence of the third MRG-like gyre. However, the simulated relative locations of the Rossby gyres, TC05A, and the MRG-like gyres have biases.

In summary, the CTL run reproduces realistic large-scale mean circulation during the MJO and TC05A lifespan, including the mean precipitation, the northern IO winter monsoon, the southern IO trades, the SWIO convergence zone, the MJO-related Rossby gyres and equatorial westerlies, and the seedling MRG-like of TC05A. The CTL run also simulates reasonable extreme precipitation events caused by the SWIO convergence zone, the convective Rossby gyres associated with the MJO, and TC05A (especially at the rapid intensification stage). The MJO propagation is well represented by the Hovmoller diagram of precipitation (Figure 3), but there is a wet bias in the MJO suppressed phase. The daily evolution of TC05A and the accompanied multiscale features of the MJO and MRG-like gyres are generally well represented in the CTL run. This adds confidence to further sensitivity experiments.

4. Results From the PLF Experiments

To investigate impacts of the SY, IS, and IA forcings on the multiscale interaction dynamics during the TC05A lifespan, we examine the differences between the CTL experiment and the corresponding sensitivity experiments of Exp_noSY, Exp_noIS, and Exp_noIA. The difference between the CTL and Exp_noSY (CTL minus Exp_noSY) is considered as the impact of the synoptic forcing.

4.1. Impacts of Multiscale Forcing on the Weekly Mean Circulation

To obtain an overall view, we first, in Figure 6, examine the impacts of different time scale forcings on a weekly (23–30 November) mean low-level circulation and precipitation. The ERA-Interim analysis shows that an anomalous cyclonic pattern that occupies the entire Arabian Sea overlaps a significant negative geopotential height anomaly. This anomalous cyclone contains the anomalies caused jointly by the TC05A activity and the northern Rossby gyre associated with the MJO (Figure 6a). The anomalies of ERA-Interim are derived

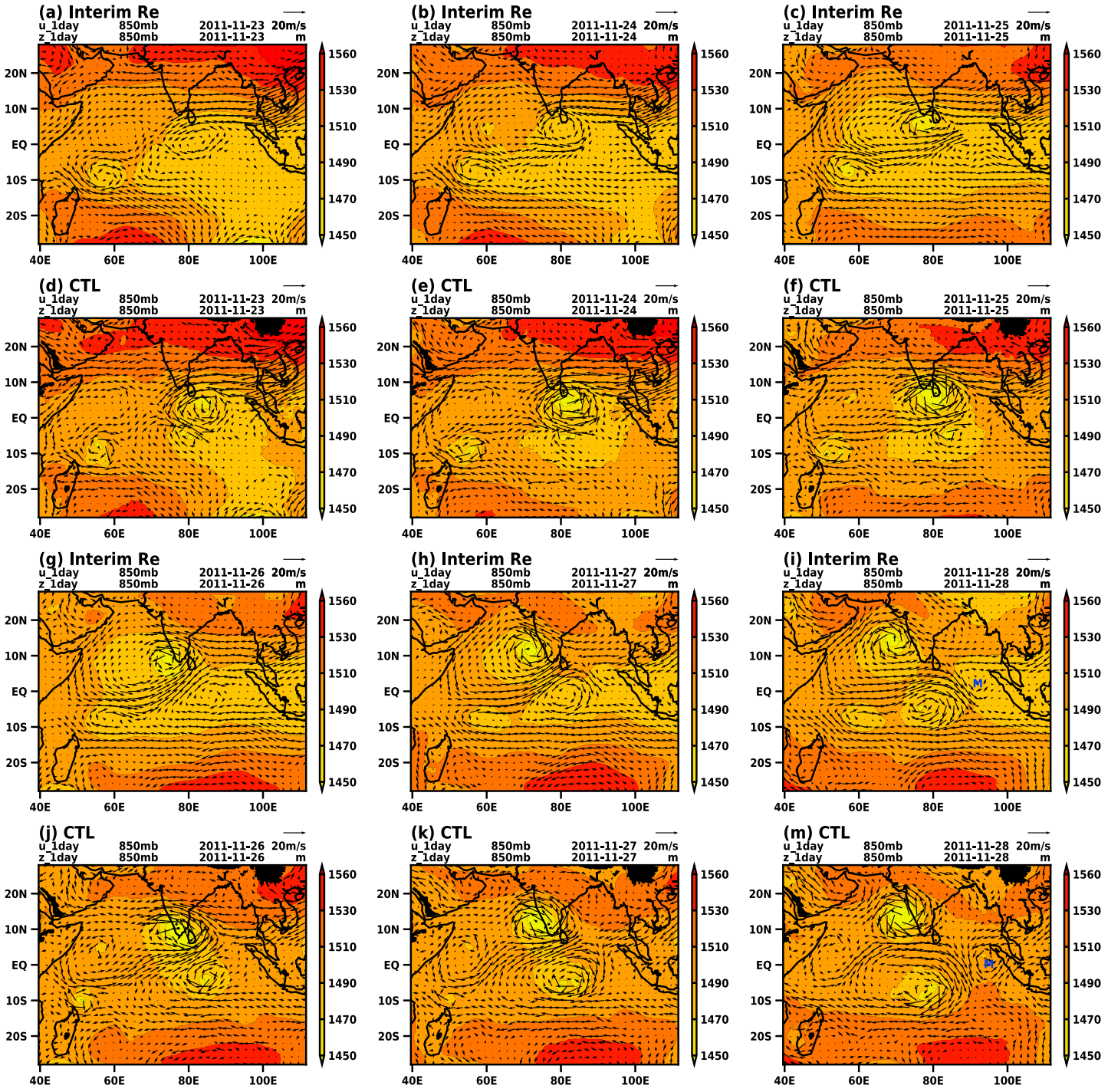

Figure 5. Daily geopotential height (shading in units of meter) and horizontal winds (vector in units of m/s) at 850 hPa during 23 to 28 November obtained from ERA-Interim (a–c, g–i) and the CTL experiment (d–f, j–m), respectively. Black masked area is the area where the topography is higher than 850 hPa. CTL = control.

from the data between 1979 and 2013. Correspondingly, significant positive vorticity anomaly occurs along the path of TC05A (Figure 6b). Note that the southern edge of this cyclonic pattern extends to the south of the equator; thus, precipitation is unfavorable on the SH side. It is indicated with red crosses in Figure 6b. The southern Rossby gyre over the southwestern IO enhances rainfall. A negative geopotential height anomaly caused by the TD developed from the second MRG-like gyre (Figure 5g) is significant over the SH around 80°E, where the rainfall is increased.

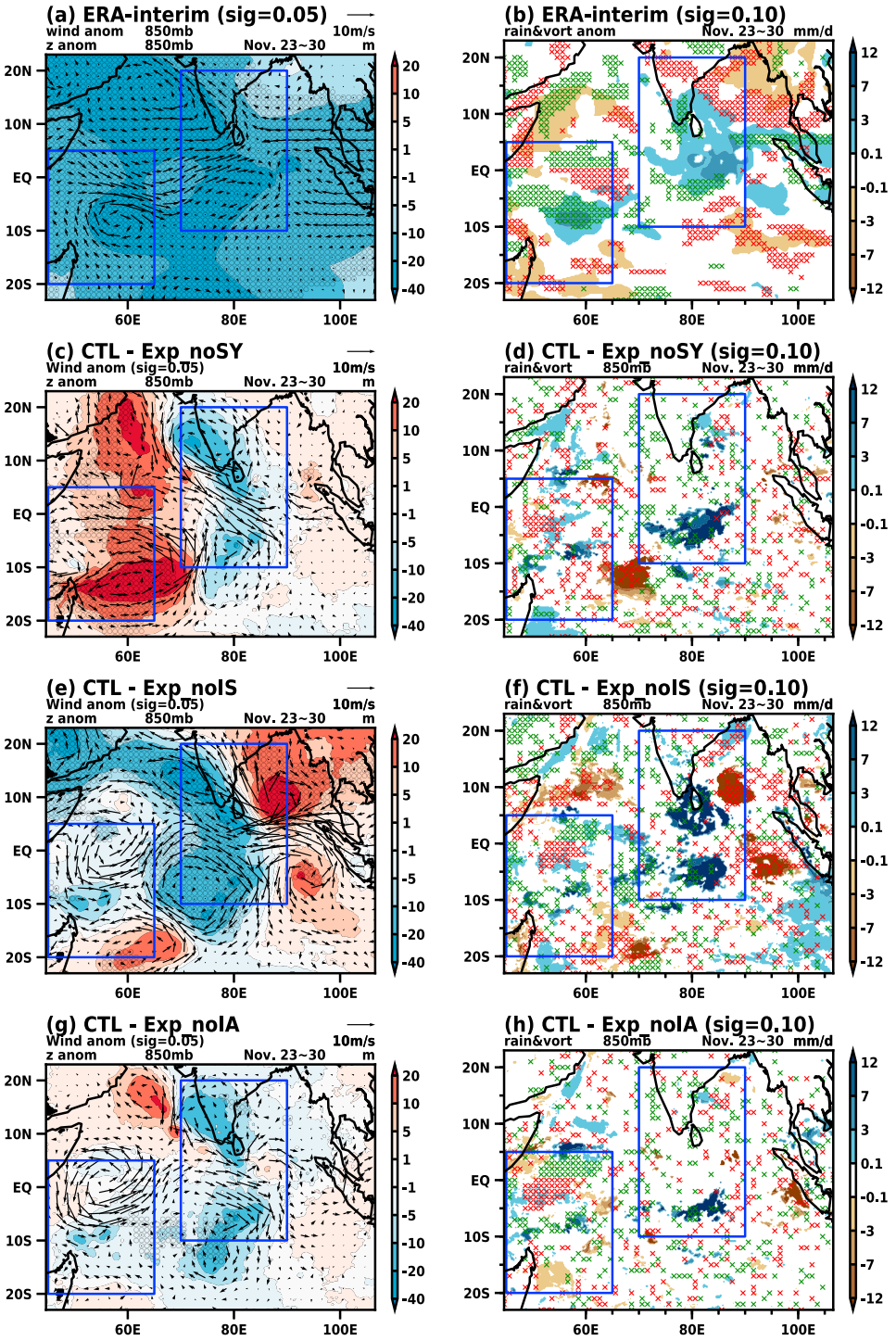

Figure 6. Impacts of multi–time scale forcing on weekly mean (from 23 to 30 November) anomalies. Figure 6a demonstrates anomalous geopotential height and horizontal wind of ERA-Interim on 850 hPa. Figures 6c, 6e, and 6g show differences in geopotential height and horizontal wind on 850 hPa between the CTL and the sensitivity experiments of Exp_noSY, Exp_noIS, and Exp_noIA, respectively. Geopotential height is shaded in units of meters, and vectors present horizontal wind in units of m/s. The hatch of black circle indicates the area where the geopotential height is significantly changed at the 95% confidence level by the Student's *t* test. Figure 6b shows significant anomalies in rainfall and 850-hPa relative vorticity of ERA-Interim. Figures 6d, 6f, and 6h show significant differences in rainfall and 850-hPa relative vorticity between the CTL and the three sensitivity experiments. Rainfall anomaly is shaded in units of mm/day. Vorticity anomaly is marked with cross hatch, where the green cross represents positive (negative) vorticity in the NH (SH) and red cross represents negative (positive) vorticity in the NH (SH). Therefore, the green cross indicates the vorticity anomaly favorable for precipitation while the red one does not. The anomalies of rainfall and vorticity pass the Student's *t* test with significance at the 90% confidence level. The anomalies of ERA-Interim are derived from the data between 1979 and 2013. Blue boxes indicate the region of dWest and dMiddle defined in Figure 1. CTL = control; NH = Northern Hemisphere; SH = Southern Hemisphere.

Figure 6c shows that the SY forcing contributes to TC05A, which is evidenced by the cyclonic circulation anomaly over the southern tip and west coast of India. However, the contribution of the SY forcing to TC05A is only significant in terms of positive vorticity (Figure 6d). Furthermore, with significant positive rainfall and negative vorticity anomalies, the SY forcing contributes to the TD over the SH developed from the second MRG-like gyre (Figure 5g). On the other hand, the SY forcing does not contribute to the anomalies caused by the Rossby gyres associated with the MJO (Figure 6a). Instead, it produces anticyclones in both hemispheres and equatorial easterly over the west IO. The anticyclones and equatorial easterly offset part of the MJO signal.

Figure 6e shows that the IS forcing contributes significantly to the anomalies caused by both Rossby gyres associated with the MJO (Figure 6a). It is evidenced by negative geopotential height (but only over small areas), positive rainfall, and positive (negative) vorticity over the Northern Hemisphere (SH) Figure 6f). Since there is a shift of the Rossby gyres in the CTL experiment, the contribution of the IS forcing to the Rossby gyres exhibits similar locational shifts. As to TC05A, the IS forcing creates significant negative geopotential height (Figure 6e) and positive vorticity anomalies (Figure 6f), as well as rainfall anomaly at the genesis location of TC05A (Figure 6f). Nevertheless, the IS forcing also helps the TD over the SH developed from the second MRG-like gyre by generating consistent positive rainfall and negative geopotential height and vorticity anomalies. The IS forcing produces a pair of anticyclones straddling the equator in the eastern IO with suppressed rainfall and equatorial easterly, which resembles the low-level anticyclonic circulation of moist Kelvin mode associated with the MJO (Rui & Wang, 1990) when the MJO convective center is located east to 80°E after 23 November (Figure 3a). Together with the TC05A vortex and TD gyres over the SH, the pair of anticyclones form a Rossby-Kelvin wave couplet.

Figure 6g shows that the IA forcing has little influence on the negative height anomalies caused by the Rossby gyres, but has a significant impact on the northern Rossby gyre in terms of vorticity and rainfall on its north side (Figure 6h). As to the suppressed southern Rossby gyre, the IA forcing increases rainfall significantly and the associated cyclonic vorticity. Similar to the SY forcing, the IA forcing only influences the vorticity field associated with TC05A (Figure 6h). On the other hand, the IA forcing displays a stronger influence on the TD over the SH in all three fields.

In sum, both SY and IA forcings only enhance the vorticity field associated with TC05A but not the geopotential height and rainfall. However, the IS forcing makes significant contributions to TC05A coherently in the anomalies of all three fields. As for the TD over the SH developed from the second MRG-like gyre, the SY forcing provides significant positive contributions to rainfall and vorticity, while both the IA and IS forcings have significant impacts in all three fields. In addition, the IS forcing causes the development of a Rossby-Kelvin wave couplet associated with the MJO.

4.2. Impacts of Multiscale Forcing on the Genesis, Intensity, and Movement of TC05A

Figure 7 shows the impact of various time scale forcings on TC05A's genesis location, path, and intensity during 23–29 November. The genesis location, path, and intensity are determined by using the minimum mean sea level pressure (MSLP). For convenience, we name the vortices corresponding to TC05A in the experiments of CTL, Exp_noSY, Exp_noIS, Exp_noIA, and observation from ERA-Interim and the Joint Typhoon Warning Center (JTWC) as TC_CTL, TC_noSY, TC_noIS, TC_noIA, and TC_ERA–JTWC, respectively, deemphasizing their intensity-based TC types. The genesis of those TC-type disturbances is defined using the minimum MSLP, which is less than 1007.5 hPa. TC_CTL, TC_noSY, TC_noIS, and TC_noIA are all formed on 23 November, which can be visually confirmed in daily fields of MSLP and geopotential height (figure not shown). The observed minimum MSLP at the center of TC_ERA–JTWC is from ERA-Interim during 23–24 November and from JTWC best track data during 25–29 November. The JTWC data only have record after 25 November when the vortex strengthened to the TD category.

TC_ERA–JTWC occurs around 87°E on the equator on 23 November. It moves northwestward almost straigthforward to 16°N, 66°E on 29 November. Its central MSLP decreases below 998 hPa on 28 November. TC_CTL behaves close to TC_ERA–JTWC but with bias. TC_CTL starts around 4°N southeast to Sri Lanka on 23 November. It moves to the west and stays south of Sri Lanka for 2 days with the central MSLP decreasing below 1,000 hPa. Then it moves northwestward and passes the southern tip of India in the next 2 days. It turns to the west-northwest with decreased intensity after 27 November.

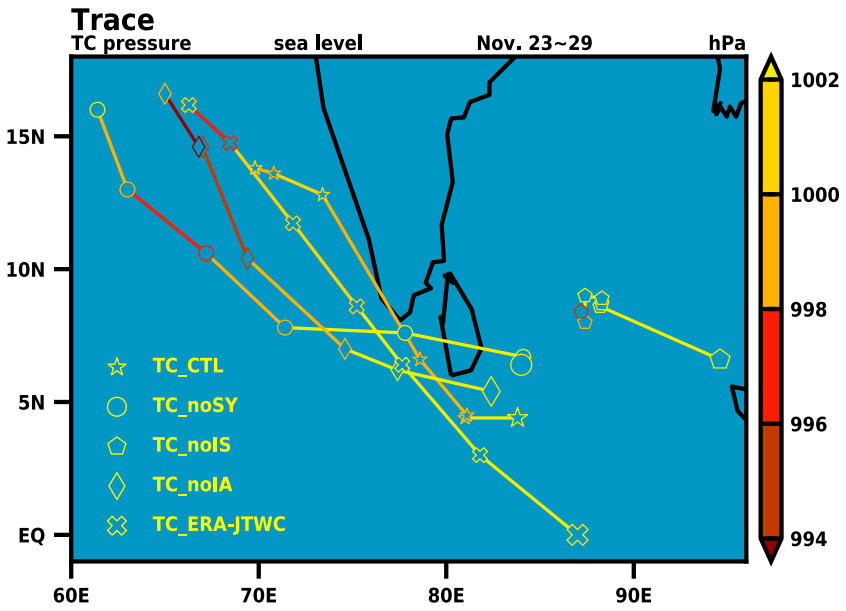

Figure 7. Impacts of multi–time scale forcing on the daily track of TC05A during 23–29 November. TC_CTL, TC_noSY, TC_noIS, TC_noIA, and TC_ERA–JTWC denote the TC-type disturbances corresponding to the TC05A in CTL, Exp_noSY, Exp_noIS, Exp_noIA, and observation, respectively. The track is determined by the location of minimum MSLP (in units of hPa). Track color denotes the intensity in terms of MSLP in vortex center. Larger marker represents the genesis location of each TC-type disturbance. The observed track is from ERA-Interim during 23–24 November and from JTWC during 25–29 November. TC = tropical cyclone; MSLP = mean sea level pressure; JTWC = Joint Typhoon Warning Center.

Both the TC_noSY and TC_noIA are initiated at a place close to and little north of TC05A. Their subsequent tracks are more westward than the path of TC_CTL. They turn northwestward with increased intensity after 26 November. The intensity reaches maximum on 27 November and then decreases. In contrast, the TC_noIS is unique. It starts in the southeast of the Bay of Bengal (BOB), far to the east of the genesis location of TC_CTL. It only rapidly moves northwestward on the first day and then spins locally around 8°N and 88°E during its later lifespan. The intensity is rapidly increased only in its final 2 days. Its track during the whole lifespan is confined in the BOB.

In sum, compared to the CTL run, both SY and IA forcings have similar, minor effects on TC05A. They shift the path of TC05A eastward to make it closer to the Indian west coast in the later stage but reduce the intensity. Different from SY and IA forcings, the IS forcing has the greatest impact on the generation and path of TC05A. It is the IS forcing that shifts the TC05A genesis location near Sri Lanka and drives it northwestward toward the Arabian Sea. In other words, it is the IS forcing that brings huge potential damage to Sri Lanka and India. If there were no IS forcing, TC05A would be generated at the eastern BOB and move to the west only in a short distance in BOB.

4.3. Impacts of Multiscale Forcing on Heavy Precipitation

Figure 8a shows that the SY forcing only causes slight rainfall anomaly before the genesis of TC05A. After 23 November, the SY forcing contributes considerable rainfall to the dMiddle through the influence on TC05A and the TD in the SH (Figure 5g). After TC05A moves out of the dMiddle from the west boundary, rainfall starts to decrease. Similar to the SY forcing, the IA forcing also slightly increases rainfall before the genesis of TC05A; it produces favorable circulation patterns to promote the development of TC05A and the TD in the SH, which causes wet anomalies mainly after 23 November. However, the IA forcing has a small influence on the rainfall of the dMiddle compared to the SY and IS forcings.

Before 18 November, the IS forcing produces dry anomalies to the dMiddle (Figure 8b), which is caused by the anomalous anticyclonic circulation traveling to the west in both hemispheres (figure not shown). Following the anomalous anticyclones, a MRG-like disturbance forms on the equator and travels westward into the dMiddle, which causes wet anomalies after 18 November. After 23 November, the MRG-like

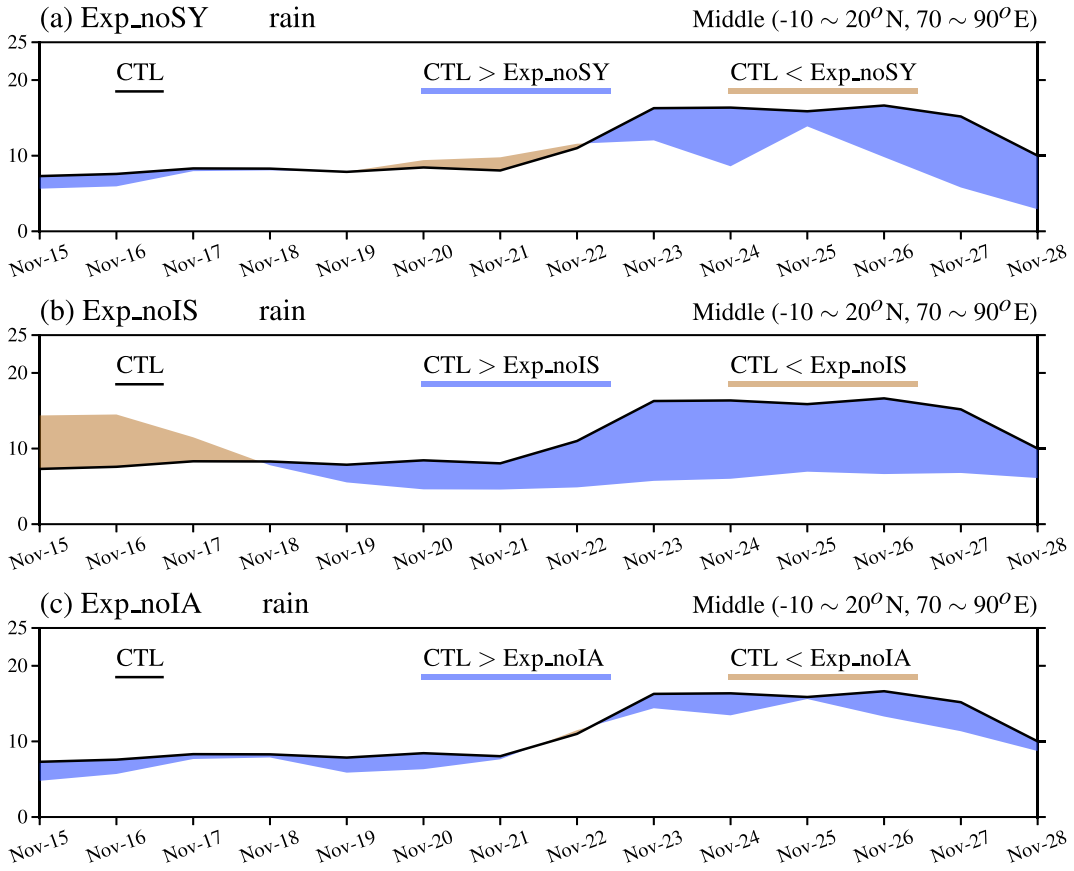

Figure 8. Impacts of multi–time scale forcing on precipitation in the dMiddle. The area-averaged daily precipitation (mm/day) in the CTL experiment (solid black curve) and its differences (colors) from the sensitivity experiments of (a) Exp_noSY, (b) Exp_noIS, and (c) Exp_noIA are shown. Blue (brown) color indicates that the precipitation in the CTL is more (less) than that in the sensitivity experiment. CTL = control.

disturbance is strengthened and gradually shifts northward, becoming TC05A. Meanwhile, the second MRG-like convection gyre forms and gradually shifts to the SH, becoming a TD. The northern TC05A and the southern TD resemble a pair of convective gyres straddling the equator though they are not at the same longitude. After 27 November, the divergent flow east of the convective gyres induces a pair of anticyclonic patterns that are associated with a Kelvin-like wave (Figure 6), which begins to decrease the wet anomaly in the dMiddle (Figure 8b). The pair of convective gyres and the pair of anticyclonic gyres to its east resemble a Rossby-Kelvin wave couplet associated with the MJO. In brief, if there were no IS forcing, the corresponding TC_noIS could only contribute to rainfall near the eastern boundary of the dMiddle (Figure 7).

In summary, the SY and IA forcings produce rainfall in the dMiddle mainly through their contributions to TC05A and the TD-type disturbance, but the effect of the IA forcing is much less. The IS forcing produces a large MRG-like gyre which later develops into TC05A then induces a Rossby-Kelvin wave couplet associated with the MJO and therefore causes heavy rainfall in the dMiddle.

5. How the Intraseasonal Forcing Influences TC05A

In the previous section, the effects of the SY, IS, and IA forcings in the LB on TC05A are studied. Previous studies show that the underlying SST anomaly is strongly coupled to the November MJO event (Fu et al., 2015; Wang et al., 2015) and important to TC05A. This aspect and related topics need further studies, which are beyond the scope of the present study. Except the SST anomaly, the IS forcing is found to be the key factor that dominates TC05A, the MJO, and their interaction. The LB IS forcing is the only forcing that drives TC05A

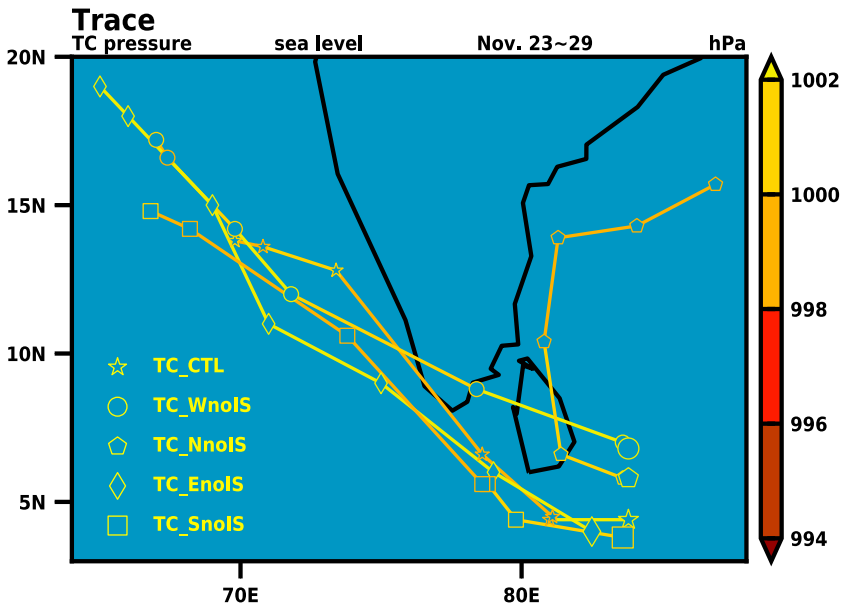

Figure 9. Impacts of different sources of the IS forcing on daily track of TC05A during 23–29 November. TC_CTL, TC_WnoIS, TC_NnoIS, TC_EnoIS, and TC_SnoIS denote the TC-type disturbances corresponding to the observed TC05A in CTL, Exp_WnoIS, Exp_NnoIS, Exp_EnoIS, and Exp_SnoIS, respectively. The track is determined by the location of minimum MSLP (in units of hPa). Trace color denotes the intensity in terms of MSLP in vortex center. Larger marker represents the genesis location of each TC-type disturbance. IS = intraseasonal; TC = tropical cyclone; CTL = control; MSLP = mean sea level pressure.

to pass the coast of Sir Lanka and India, which induces huge damages. Thus, in this section, we are motivated to investigate where the IS forcing comes from: the South IO, Africa, the Maritime Continent, or the northern lands. We design four additional sensitivity experiments of Exp_WnoIS, Exp_NnoIS, Exp_EnoIS, and Exp_SnoIS to examine the impact of the IS forcing through each of the four LBs. The tracks of the vortex corresponding to TC05A in the sensitivity experiments of Exp_WnoIS, Exp_NnoIS, Exp_EnoIS, and Exp_SnoIS are shown in Figure 9 and named as TC_WnoIS, TC_NnoIS, TC_EnoIS, and TC_SnoIS, respectively.

5.1. Impacts of the IS Forcing on the Genesis, Intensity, and Movement of TC05A

The TC_NnoIS starts about 1.5° of latitude to the north of the genesis location of TC_CTL. It stays there for 2 days and then travels northwestward to hit the southeastern coast of Sri Lanka. On 25 November, it suddenly turns northward, going across Sri Lanka. After 26 November, it increases the intensity and later turns right for almost 90°, traveling again toward the east. The absence of northern boundary IS forcing dramatically changes the TC05A life cycle. In sharp contrast, the TC_SnoIS is initiated slightly south of the TC_CTL genesis location. The path of TC_SnoIS is very similar to that of the TC_CTL except that it slightly shifts to the south, suggesting that the IS forcing from the southern LB does not significantly affect TC05A.

The TC_WnoIS is initiated east of Sri Lanka and about 2° of latitude to the north of the genesis location of TC_CTL. It stays there for 2 days and then rapidly travels northwestward, crossing Sri Lanka and the southern Indian tip. It slows down and intensifies on 28 November before it finally decreases the strength. Thus, the IS forcing from the western LB mainly shifts the genesis location northward and slows down the northwestward propagation of TC05A. The TC_EnoIS forms slightly southwest to the genesis location of TC_CTL. It quickly moves northwestward to the Arabian Sea. During its lifespan, TC_EnoIS travels the longest distance without strong intensification. In comparison with the CTL run, the eastern IS forcing slows down TC05A and increases its intensity.

In sum, compared with the CTL run, the northern boundary IS forcing has the greatest impact on the path of TC05A. It is the main factor that causes the prominent steering flow that drivers TC05A to move northwestward and cross the southern tip of India to the Arabian Sea. Therefore, the northern IS forcing is the main driver that brings the damage to the southern coast of Sri Lanka and the southern and southwestern coasts of

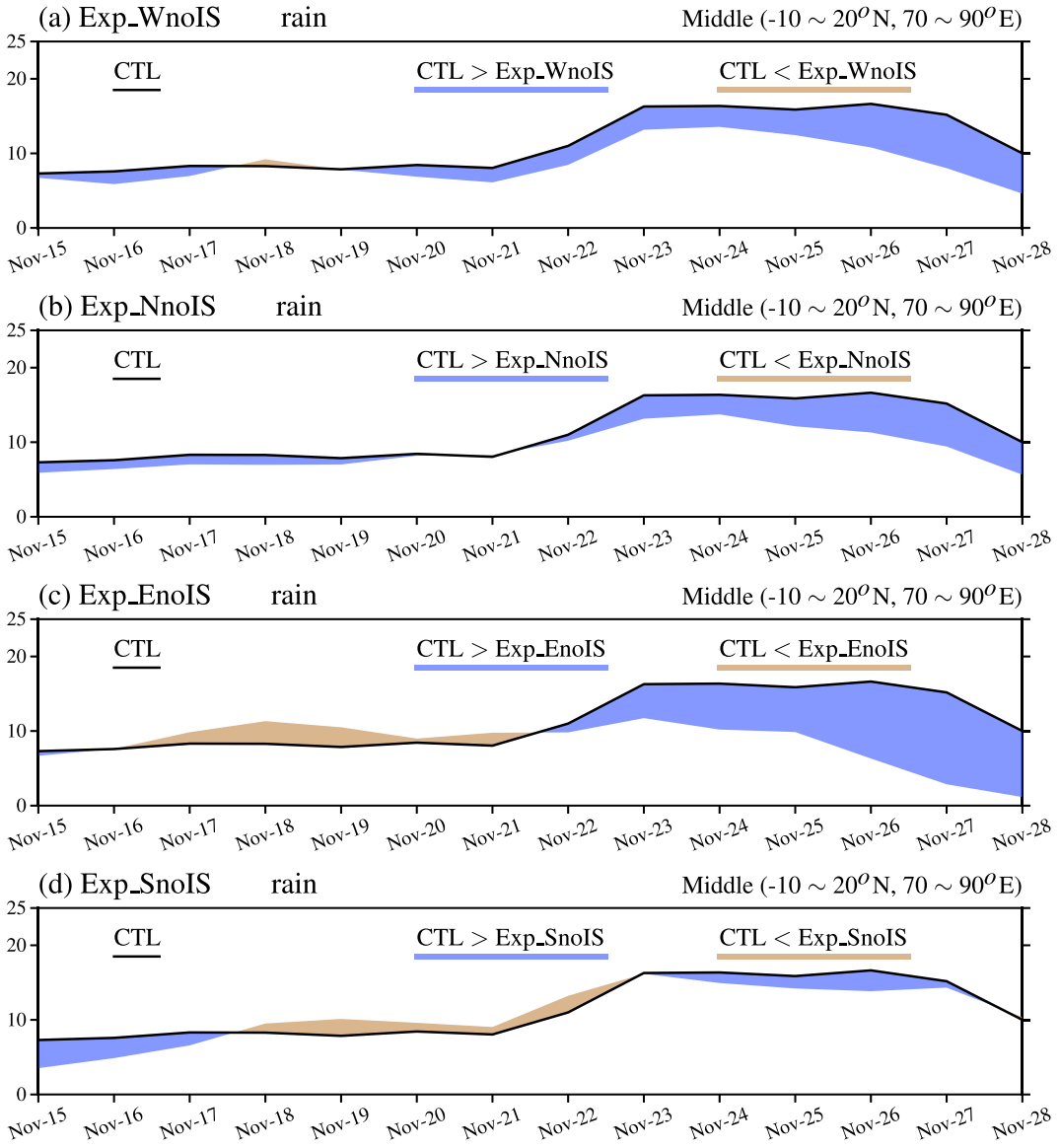

Figure 10. Impacts of different sources of the IS forcing on precipitation in the dMiddle. The area-averaged daily precipitation (mm/day) in the CTL (solid black curve) and its differences (colors) from the sensitivity experiments of (a) Exp_WnoIS, (b) Exp_EnoIS, (c) Exp_SnoIS, and (d) Exp_NnoIS are shown. Blue (brown) color indicates that the precipitation in the CTL is more (less) than that in the sensitivity experiment. IS = intraseasonal; CTL = control.

India. The western IS forcing slows down TC05A and drives the track more equatorward. The eastern IS forcing increases the intensity of TC05A and slows it down. The southern IS forcing is unimportant.

5.2. Impacts of the IS Forcing on Heavy Rainfall

Figure 10 shows the impact of the IS forcing from individual LB on the rainfall mainly associated with TC05A. Figure 10a shows that the western IS forcing causes wet anomalies in most of the time. The less precipitation in Exp_WnoIS after 24 November is caused by the faster speed of TC_WnoIS relative to the TC_CTL so that the TC_WnoIS moves away from the dMiddle 2 days earlier than the TC_CTL (Figure 9). The northern IS forcing causes wet anomaly in the dMiddle, similar to that caused by the western IS forcing (Figure 10b). However, their mechanisms are different. In contrast to the Exp_WnoIS, the dry anomaly in Exp_NnoIS is mainly caused by the absence of the second MRG-like convection gyre in the dMiddle: the corresponding MRG-like gyre in Exp_NnoIS shifts eastward out of the dMiddle, following the track of TC_NnoIS (figure not shown).

In the experiment Exp_EnoIS, the northern Rossby gyre associated with the MJO is located east of its original place (figure not shown), which causes some rainfall in the dMiddle at the early stage (Figure 10c). The less rainfall in Exp_EnoIS after 23 November is caused by the faster northwestward movement of TC_EnoIS relative to TC_CTL (Figure 9), which makes TC_EnoIS leave the dMiddle earlier. On the other hand, the TC_CTL passes over the coastline so that relatively more rainfall in the CTL run may be affected by the complex terrain effect (Chang et al., 2013). In addition, the less rainfall in Exp_EnoIS is also related with the weaker intensity of TC_EnoIS, which is relatively far from the land (Jiang et al., 2008; Lonfat et al., 2004; Yu et al., 2017). The TC_SnoIS evolves similarly to TC_CTL (Figure 9). Consequently, only the southern IS forcing causes small rainfall anomaly (Figure 10d).

In summary, the eastern IS forcing has the greatest contribution to the rainfall associated with TC05A in the dMiddle. The IS forcing from western and northern LBs has a moderate impact on TC05A rainfall. The southern IS forcing has a negligible impact.

6. Conclusion and Discussion

The TC05A caused huge damage to Sri Lanka and India in November 2011. Using the data obtained from the Intensive Observing Period of the DYNAMO field campaign, many studies have focused on TC05A (Fu et al., 2013; Gottschalck et al., 2013; Moum et al., 2014). However, as a very interesting case of TC-MJO interaction, the multiscale interactive processes among SY, IS, and IA variations remain elusive.

Our CTL experiment demonstrates that the WRF model is capable of reproducing the mean circulation and precipitation, MJO structure and propagation, and the genesis and track of TC05A as well as other major synoptic systems over the IO during the late part of November 2011, including the location and evolution of the heavy rainfall induced by TC05A. However, the CTL experiment has a wet bias during the MJO suppressed phase.

A set of sensitivity experiments is designed to identify the effects of the SY, IS, and IA forcings in the LB on TC05A. Results show that the IS forcing has the greatest impact on TC05A, especially on its heavy precipitation when it rapidly intensifies. While both the SY and IA forcings also contribute to the cyclonic vorticity genesis of TC05A, it is the IS forcing that realistically reproduces the coherent fields that are favorable for the development of TC05A, including the atmospheric humidity, low-level convergence, and the cyclonic vorticity. The IS forcing plays an important role in determining the location of TC05A genesis, resulting in TC genesis near Sri Lanka in the BOB and the northwestward motion to the Arabian Sea. This causes huge damages in the coasts of Sri Lanka and India. This process involves the MJO-induced MRG-like gyre, which develops into TC05A. The IS component contributes the Rossby-Kelvin wave couplet to the low-level circulation. Without the cyclone and anticyclone pair of the Rossby-Kelvin wave couplet in the Northern Hemisphere, TC05A would be shifted half wave length eastward to the eastern BOB and confined in the BOB during the whole lifespan.

Since the IS forcing exerts the most important impacts on TC05A and the MJO as well as their interaction, we design another set of sensitivity experiments in which the IS forcing is individually removed from the eastern, southern, western, and the northern LB, in order to identify the source of the IS forcing that is most influential on TC05A. Results show that the northern LB IS forcing has the greatest impact on the genesis location and path of TC05A. It is the main driver that leads TC05A northwestward to cross the south tip of India to the Arabian Sea, therefore causing huge damage to the southern coast of Sri Lanka and the southern and southwestern coasts of India. The western LB IS forcing tends to slow down TC05A and deviates it equatorward. The eastern LB IS forcing favors increasing the TC intensity and slowing down TC05A, contributing to the heavy rainfall in the central IO, Sri Lanka, and India. The southern LB IS forcing is unimportant. Remember that the contribution of the IS forcing from four sides of LB together forms the Rossby-Kelvin wave couplet, while the IS forcing from an individual side does not contribute to such an idealized pattern. The interaction of signals from four sides is nonlinear, thus the genesis location of TC in experiment without IS forcing on four sides is not a linear combination of the genesis locations in the four experiments without IS forcing on each side. Therefore, the genesis location of TC05A would not be shifted to the eastern BOB by any individual LB IS forcing.

Previous studies have confirmed that the interaction among the convective phases of an ER or a TD-like wave, a Kelvin wave, and the MJO leads to the genesis of TC05A (Gottschalck et al., 2013). Here we show evidences

suggesting that a MJO-MRG interaction leads to the genesis of TC05A. The pressure field of the MRG-like gyre on 23 November (Figure 5a) is asymmetric about the equator, possibly due to the mean flow effects: the northeasterly winter monsoon flows prevail from the South China Sea to the northern IO. In theory, the mean flows can have significant impacts on the equatorial waves. Wang and Xie (1996) and Xie and Wang (1996) have extended the Matsuno theory by inclusion of mean flow effects. The presence of the vertical wind shear of the mean flow can significantly change the wave structure, especially the ER wave. How mean flow affects MRG waves calls for further study. After the first MRG-like wave moves northward and becomes TC05A, the second MRG-like wave occurs and moves to the SH and becomes a TD. These two convective gyres are similar to a pair of ER gyres but are not at the same longitude. Surprisingly, we have found that it is not the equatorial synoptic easterly waves that cause the northwestward movement of TC05A from the BOB to the Arabian Sea. Rather, it is the effect of the IS forcing from the northern LB that prominently influences the track of TC05A. It suggests the importance of the MJO interaction with Northern Hemisphere winter monsoon for the track of TC05A. The northern IS forcing is embedded in the boreal monsoon flow, which steers low-level anticyclonic wind systems westward and provides the basic flows that promote TC05A to move northwestward from the BOB to the northern Arabian Sea.

Our study has limitations. Since the MJO is a coupled atmosphere-ocean phenomenon to a certain extent, time-varying SST plays an important role in numeric simulation of the November MJO event (Wang et al., 2015). A coupled model might be relatively appropriate than the approach that we used in this study; that is, the prescribed time varying SST is used as the underlying boundary condition for the WRF model. However, as long as the approach fits the objective of this study, it could be acceptable. Previous studies (Wang et al., 2015) showed that using the WRF model with a prescribed daily varying SST instead of using coupled model could reasonably simulate the November MJO event, even though the November MJO event interacted with the underlying ocean much stronger than the October MJO event (Fu et al., 2015). We did not assess the bias (Figure 4) or contribution (Figures 8 and 10) due to the time lag of TC genesis between the CTL, sensitivity experiments and observations. Since the time lag may change the bias or contribution, the bias in temporal dimension should not be neglected. This study focuses on the impacts of multiscale forcings (synoptic, intraseasonal, and interannual) on TC genesis, track, and rainfall. The associated mesoscale dynamics, such as warm core formation and moisture aggregations, calls for a future study.

Appendix A: Acronyms

List of Select Acronyms

BOB	Bay of Bengal
CAM	Community Atmospheric Model
CMORPH	Climate Prediction Center Morphing Technique
CTL	Control
DYNAMO	Dynamics of the MJO
ER	Equatorial Rossby
ERA	European Centre for Medium–Range Weather Forecasts Reanalysis
IA	Interannual
IO	Indian Ocean
IOD	IO Dipole
IS	Intraseasonal
JTWC	Joint Typhoon Warning Center
LB	Lateral boundary
MJO	Madden–Julian Oscillation
MRG	Mixed Rossby–Gravity
MSLP	Mean sea level pressure
PLF	Partial lateral forcing
SH	Southern Hemisphere
SST	Sea surface temperature
SSTA	SST anomaly
SWIO	Southwestern IO

SY	Synoptic
TC	Tropical cyclone
TD	Tropical depression
WRF	Weather Research and Forecast
WWB	Westerly wind burst

Acknowledgments
The first author Hongwei Yang acknowledges the support from the APEC Climate Center (APCC). Bin Wang acknowledges the support by the U.S. NOAA ESS award NA13OAR4310167 and NSF award AGS-1540783. It is Publication 214 of the Earth System Modeling Center. The authors would like to thank four anonymous reviewers and the Editor for their constructive and insightful comments. The ERA-Interim data set was obtained from ECMWF (https://www.ecmwf.int/en/research/climate-reanalysis/era-interim). CMORPH data were obtained from CPC (http://www.cpc.ncep.noaa.gov/products/janowiak/cmorph_description.html), and the WRF model was from NCAR (http://www2.mmm.ucar.edu/wrf/users/download/get_source.html). The experimental results computed by using WRF are available in an online repository (https://figshare.com/articles/data_tar_gz/5959978).

References

Aiyyer, A. R., & Molinari, J. (2003). Evolution of mixed Rossby–gravity waves in idealized MJO environments. *Journal of the Atmospheric Sciences*, *60*, 2837–2855.

Bessafi, M., & Wheeler, M. C. (2006). Modulation of South Indian Ocean tropical cyclones by the Madden-Julian oscillation and convectively coupled equatorial waves. *Monthly Weather Review*, *134*, 638–656.

Camargo, S. J., Wheeler, M. C., & Sobel, A. H. (2009). Diagnosis of the MJO modulation of tropical cyclogenesis using an empirical index. *Journal of the Atmospheric Sciences*, *66*, 3061–3074.

Chang, C.-P., Yang, Y.-T., & Kuo, H.-C. (2013). Large increasing trend of tropical cyclone rainfall in Taiwan and the roles of terrain. *Journal of Climate*, *26*, 4138–4147.

Chen, F., & Dudhia, J. (2001). Coupling an advanced land surface-hydrology model with the Penn State-NCAR MM5 modeling system. Part I: Model implementation and sensitivity. *Monthly Weather Review*, *129*, 569–585.

Chen, G., & Chou, C. (2014). Joint contribution of multiple equatorial waves to tropical cyclogenesis over the western North Pacific. *Monthly Weather Review*, *142*, 79–93.

Collins, W. D., Rasch, P. J., Boville, B. A., Hack, J. J., McCaa, J. R., Williamson, D. L., et al. (2004). Description of the NCAR community atmosphere model (CAM 3.0). Technical Report National Center for Atmospheric Research

Dee, D. P., Uppala, S. M., Simmons, A. J., Berrisford, P., Poli, P., Kobayashi, S., et al. (2011). The ERA-Interim reanalysis: Configuration and performance of the data assimilation system. *Quarterly Journal of the Royal Meteorological Society*, *137*, 553–597.

Dickinson, M., & Molinari, J. (2002). Mixed Rossby-gravity waves and western Pacific tropical cyclogenesis. Part I: Synoptic evolution. *Journal of the Atmospheric Sciences*, *59*, 2183–2196.

Emanuel, K., & Nolan, D. S. (2004). *Tropical cyclone activity and global climate*. Paper presented at Proc. 26th Conf. on Hurricanes and Tropical Meteorology, Miami, FL.

Fu, X., & Hsu, P.-C. (2011). Extended-range ensemble forecasting of tropical cyclogenesis in the northern Indian Ocean: Modulation of Madden-Julian oscillation. *Geophysical Research Letters*, *38*, L15803. https://doi.org/10.1029/2011GL048249

Fu, X., Lee, J.-Y., Hsu, P.-C., Taniguchi, H., Wang, B., Wang, W., & Weaver, S. (2013). Multi-model MJO forecasting during DYNAMO/CINDY period. *Climate Dynamics*, *41*, 1067–1081.

Fu, X., Wang, W., Lee, J.-Y., Wang, B., Kikuchi, K., Xu, J., et al. (2015). Distinctive roles of air–sea coupling on different MJO events: A new perspective revealed from the DYNAMO/CINDY field campaign. *Monthly Weather Review*, *143*, 794–812.

Fudeyasu, H., Wang, Y., Satoh, M., Nasuno, T., Miura, H., & Yanase, W. (2010). Multiscale interactions in the life cycle of a tropical cyclone simulated in a global cloud-system-resolving model. Part I: Large-scale and storm-scale evolutions. *Monthly Weather Review*, *138*, 4285–4304.

Gottschalck, J., Roundy, P. E., Schreck, C. J. III, Vintzileos, A., & Zhang, C. (2013). Large-scale atmospheric and oceanic conditions during the 2011–12 DYNAMO field campaign. *Monthly Weather Review*, *141*, 4173–4196.

Hall, J. D., Matthews, A. J., & Karoly, D. J. (2001). The modulation of tropical cyclone activity in the Australian region by the Madden-Julian Oscillation. *Monthly Weather Review*, *129*, 2970–2982.

Hogsett, W., & Zhang, D.-L. (2010). Genesis of Typhoon Chanchu (2006) from a westerly wind burst associated with the MJO. Part I: Evolution of a vertically tilted precursor vortex. *Journal of the Atmospheric Sciences*, *67*, 3774–3792.

Hong, S.-Y., Noh, Y., & Dudhia, J. (2006). A new vertical diffusion package with an explicit treatment of entrainment processes. *Monthly Weather Review*, *134*, 2318–2341.

Huang, P., Chou, C., & Huang, R. (2011). Seasonal modulation of tropical intraseasonal oscillations on tropical cyclone geneses in the western North Pacific. *Journal of Climate*, *24*, 6339–6352.

Janjic, Z. I. (1994). The step-mountain eta coordinate model: Further developments of the convection, viscous sublayer, and turbulence closure schemes. *Monthly Weather Review*, *122*, 927–945.

Janjic, Z. I. (2000). Comments on "Development and Evaluation of a Convection Scheme for Use in Climate Models". *Journal of the Atmospheric Sciences*, *57*, 3686.

Jiang, H., Halverson, J. B., & Simpson, J. (2008). On the differences in storm rainfall from Hurricanes Isidore and Lili. Part I: Satellite observations and rain potential. *Weather and Forecasting*, *23*, 29–43.

Joyce, R. J., Janowiak, J. E., Arkin, P. A., & Xie, P. (2004). CMORPH: A method that produces global precipitation estimates from passive microwave and infrared data at high spatial and temporal resolution. *Journal of Hydrometeorology*, *5*, 487–503.

Klotzbach, P. J. (2010). On the Madden-Julian oscillation–Atlantic hurricane relationship. *Journal of Climate*, *23*, 282–293.

Lau, N.-C., & Nath, M. J. (2003). Atmosphere-ocean variations in the Indo-Pacific sector during ENSO episodes. *Journal of Climate*, *16*, 3–20.

Lau, W. K.-M., & Waliser, D. E. (Eds.) (2012). *Intraseasonal Variability in the Atmosphere–Ocean Climate System* (2nd ed.). Berlin: Springer.

Liebmann, B., Hendon, H. H., & Glick, J. D. (1994). The relationship between tropical cyclones of the western Pacific and Indian Oceans and the Madden-Julian oscillation. *Journal of the Meteorological Society of Japan*, *72*, 401–412.

Lonfat, M., Marks, F. D. Jr., & Chen, S. S. (2004). Precipitation distribution in tropical cyclones using the Tropical Rainfall Measuring Mission (TRMM) microwave imager: A global perspective. *Monthly Weather Review*, *132*, 1645–1660.

Madden, R. A., & Julian, P. R. (1994). Observations of the 40–50-day tropical oscillation-A review. *Monthly Weather Review*, *122*, 814–837.

Maloney, E. D., & Hartmann, D. L. (2000). Modulation of hurricane activity in the Gulf of Mexico by the Madden-Julian oscillation. *Science*, *287*, 2002–2004.

McPhaden, M. J., Wang, Y., & Ravichandran, M. (2015). Volume transports of the Wyrtki jets and their relationship to the Indian Ocean dipole. *Journal of Geophysical Research: Oceans*, *120*, 5302–5317. https://doi.org/10.1002/2015JC010901

Mo, K. C. (2000). The association between intraseasonal oscillations and tropical storms in the Atlantic basin. *Monthly Weather Review*, *128*, 4097–4107.

Moum, J. N., de Szoeke, S. P., Smyth, W. D., Edson, J. B., DeWitt, H. L., Moulin, A. J., et al. (2014). Air-sea interactions from westerly wind bursts during the November 2011 MJO in the Indian Ocean. *Bulletin of the American Meteorological Society*, *95*, 1185–1199.

Rui, H., & Wang, B. (1990). Development characteristics and dynamic structure of tropical intraseasonal convection anomalies. *Journal of the Atmospheric Sciences*, *47*, 357–379.

Schreck, C. J. III (2015). Kelvin waves and tropical cyclogenesis: A global survey. *Monthly Weather Review*, *143*, 3996–4011.

Schreck, C. J. III, Molinari, J., & Aiyyer, A. (2012). A global view of equatorial waves and tropical cyclogenesis. *Monthly Weather Review*, *140*, 774–788.

Skamarock, W. C., Klemp, J. B., Dudhia, J., Gill, D. O., Barker, M., Duda, K. G., et al. (2008). A description of the advanced research WRF Version 3. Technical Report National Center for Atmospheric Research

Thompson, G., Field, P. R., Rasmussen, R. M., & Hall, W. D. (2008). Explicit forecasts of winter precipitation using an improved bulk microphysics scheme. Part II: Implementation of a new snow parameterization. *Monthly Weather Review*, *136*, 5095–5115.

Wang, B., & Moon, J.-Y. (2017). An anomalous genesis potential index for MJO modulation of tropical cyclones. *Journal of Climate*, *30*, 4021–4035.

Wang, B., & Rui, H. (1990). Dynamics of the coupled moist Kelvin-Rossby wave on an equatorial β-plane. *Journal of the Atmospheric Sciences*, *47*, 397–413.

Wang, B., & Xie, X. (1996). Low-frequency equatorial waves in vertically sheared zonal flow. Part I: Stable waves. *Journal of the Atmospheric Sciences*, *53*, 449–467.

Wang, B., & Zhou, X. (2008). Climate variation and prediction of rapid intensification in tropical cyclones in the western North Pacific. *Meteorology and Atmospheric Physics*, *99*, 1–16.

Wang, S., Sobel, A. H., Zhang, F., Sun, Y. Q., Yue, Y., & Zhou, L. (2015). Regional simulation of the October and November MJO events observed during the CINDY/DYNAMO field campaign at gray zone resolution. *Journal of Climate*, *28*, 2097–2119.

Woolnough, S. J., Slingo, J. M., & Hoskins, B. J. (2001). The organization of tropical convection by intraseasonal sea surface temperature anomalies. *Quarterly Journal of the Royal Meteorological Society*, *127*, 887–907.

Wu, L., & Duan, J. (2015). Extended simulation of tropical cyclone formation in the western North Pacific monsoon trough. *Journal of the Atmospheric Sciences*, *72*, 4469–4485.

Xie, X., & Wang, B. (1996). Low-frequency equatorial waves in vertically sheared zonal flow. Part II: Unstable waves. *Journal of the Atmospheric Sciences*, *53*, 3589–3605.

Xu, Y., Li, T., & Peng, M. (2014). Roles of the synoptic-scale wave train, the intraseasonal oscillation, and high-frequency eddies in the genesis of Typhoon Manyi (2001). *Journal of the Atmospheric Sciences*, *71*, 3706–3722.

Yang, H., & Wang, B. (2015). Partial lateral forcing experiments reveal how multi-scale processes induce devastating rainfall: A new application of regional modeling. *Climate Dynamics*, *45*, 1157–1167.

Yoneyama, K., Zhang, C., & Long, C. N. (2013). Tracking Pulses of the Madden-Julian Oscillation. *Bulletin of the American Meteorological Society*, *94*, 1871–1891.

Yu, Z., Wang, Y., Xu, H., Davidson, N., Chen, Y., Chen, Y., & Yu, H. (2017). On the relationship between intensity and rainfall distribution in tropical cyclones making landfall over China. *Journal of Applied Meteorology and Climatology*, *56*, 2883–2901.

Zhang, F., Taraphdar, S., & Wang, S. (2017). The role of global circumnavigating mode in the MJO initiation and propagation. *Journal of Geophysical Research: Atmospheres*, *122*, 5837–5856. https://doi.org/10.1002/2016JD025665

Zong, H., & Wu, L. (2015). Synoptic-scale influences on tropical cyclone formation within the western North Pacific monsoon trough. *Monthly Weather Review*, *143*, 3421–3433.

Erratum

In the originally published version of this paper, the title was published incorrectly.

The correct title is: "Multiscale processes in the genesis of a near-equatorial tropical cyclone during the Dynamics of the MJO Experiment: Results from partial lateral forcing experiments". This version can be considered the authoritative version.